Time-delay modulation of finite-distance organization and orbital motion in a three-bubble acoustic cluster

Lingling Zhang[1],* Xun Wang[2] and Jinfu Liang[3]

[1]School of Electronic and Information Engineering,
Suzhou University of Technology,Changshu, 215506, China

[2]State Key Laboratory of Acoustics and Marine Information, Institute of Acoustics,
Chinese Academy of Sciences, Beijing, 100190, China

[3]School of Physics and Electronic Science,
Guizhou Normal University, Guiyang 550025, China

August 24, 2026

Abstract

A time-delayed pulsation–translation model is developed to investigate finite-distance organization and orbital dynamics in a three-bubble acoustic cluster. The results show that the time-delayed interaction generally selects a larger mean inter-bubble spacing and tends to reduce spacing uniformity. Pressure and initial-radius scans further show that this spacing enlargement is robust in the examined finite-distance regime, although its magnitude depends on the driving pressure and bubble-size combination. A centroid-frame acceleration decomposition further reveals that the radial component governing spacing regulation remains of the same order of magnitude, whereas the tangential component responsible for sustained orbital motion is strongly weakened. Consequently, the cluster remains spatially bounded, but its orbital angular velocity is markedly reduced. These results show that finite sound-speed propagation mainly enlarges the selected spacing while suppressing the tangential component of the collective motion.

Keywords: acoustic bubble cluster; time-delayed coupling; finite-distance organization; orbital motion
PACS: 43.35.Ei, 47.55.dd, 43.25.Yw

1. Introduction

Acoustic cavitation refers to the activation, growth, oscillation, and collapse of pre-existing gas nuclei in a liquid under acoustic forcing [1]. When exposed to a strong acoustic field, these bubbles undergo highly nonlinear processes, including slow expansion followed by violent collapse. During collapse, extreme temperatures and pressures are generated within the bubbles [2], leading to the emission of shock waves [3,4] and the induction of high-intensity acoustic microstreaming in the surrounding liquid [5,6]. These effects induce significant physical, chemical, and biological impacts [7,8]. They underpin practical technologies such as acoustic cleaning [9,10] and fragmentation [11,12].

*Corresponding author. E-mail:zhangll@cslg.edu.cn

In these technical contexts, the formation and organization of cavitation clouds are of paramount importance. Owing to advances in experimental techniques such as high-speed imaging and holography, various cavitation cloud structures have been observed [13–17]. In addition, stable bubble clusters have been reported [18,19], in which bubbles neither coalesce nor break up under sustained acoustic forcing. More intriguingly, this stability may appear in highly ordered patterns. Shirota et al. [20], Desjouy et al. [21,22], and Bai et al. [23] observed bubbles arranging into stable arrays and exhibiting orbital motion. In these ordered structures, bubbles often maintain an approximately constant inter-bubble distance and sustain periodic translational trajectories under continuous acoustic driving. Such constant-distance motion is a typical manifestation of self-organization in cavitation clouds. In sonochemical systems, the spatial distribution and collective motion of cavitation bubbles determine where collapse, microstreaming, sonoluminescence, and chemical activity are concentrated. Therefore, understanding how bubble clusters regulate their spacing and orbital motion is important for controlling cavitation activity and improving the reproducibility of ultrasonic processes.

Theoretically, researchers have explored the possibility of forming stable bubble pairs. For instance, Doinikov [24], from the perspective of secondary forces, pointed out that second-harmonic components could lead to the formation of bound bubble pairs with stable spacing, and suggested that compressibility might enable bubbles to form stable bound pairs with spacing approximately equal to the acoustic wavelength. Subsequent studies further demonstrated that such systems can form stable bubble pairs [25] and explored the precession of microbubbles about the pressure-node plane in an intense megahertz standing wave [26]. Barbat et al. [27] showed that a binary bubble system can exhibit both bounded elliptical trajectories and unbounded hyperbolic trajectories. Pelekasis et al. [28] demonstrated that stable binary bubble configurations can arise from a dynamic equilibrium between secondary Bjerknes forces and viscous drag. In our previous study [29], we investigated constant-distance collective motion in a three-bubble system and showed that a non-collinear bubble cluster can exhibit finite-distance translation and orbital motion through nonlinear pulsation–translation coupling. These studies provide an important basis for understanding finite-distance bubble interactions. However, they are generally based on the assumption of instantaneous sound propagation.

In reality, the acoustic disturbance emitted by an oscillating bubble requires a finite time to propagate through the liquid and influence neighboring bubbles. Therefore, time delay should be incorporated into interacting-bubble models. In recent years, the importance of time-delay effects in interacting bubble systems has gradually gained attention [30–34]. Ooi et al. [35] found that introducing time delay in bubble-chain systems significantly improves the agreement between model predictions and experiments. They also showed that the smaller the bubble spacing, the more important the time-delay effect becomes. This finding suggests that, for closely spaced bubbles in cavitation clouds, accurate incorporation of finite sound-speed propagation is indispensable. Thomas et al. [36,37] systematically analyzed time-delayed bubble-interaction models and revealed the importance of time delay as a function of the size and density of a bubble cluster. Nevertheless, most existing time-delay studies have focused mainly on radial pulsation dynamics, whereas the translational motion and orbital collective dynamics of interacting bubbles under time-delay effects remain less understood.

In our recent study [38], the influence of time delay on the translational dynamics of cavitation bubbles was examined, but that work was limited to a two-bubble system. A two-bubble system can describe axial attraction, repulsion, and collective translation along a single interaction axis, but it cannot fully characterize non-collinear spacing regulation or orbital motion. By contrast, a three-bubble cluster is the minimal non-collinear unit capable of supporting both finite-distance organization and orbital dynamics, because its interaction geometry allows radial and tangential components of the interaction to coexist. Therefore, the transition from a two-bubble pair to a three-bubble cluster is not merely an

increase in bubble number, but introduces qualitatively different collective degrees of freedom. Although larger bubble clusters contain richer many-body dynamics, the present work focuses on the three-bubble cluster to isolate the basic mechanism by which time delay modulates finite-distance and orbital collective states. It should be emphasized that the constant-distance and orbital states are not created by time delay itself [29]. Rather, the present work focuses on how finite sound-speed propagation modulates these pre-existing collective states. To this end, we formulate a time-delayed pulsation–translation model for a three-bubble acoustic cluster. Centroid-frame quantities, including relative trajectories, mean inter-bubble distance, coefficient of variation, acceleration decomposition, and mean angular velocity, are then used to characterize the delay-induced modulation of spacing regulation and orbital motion.

2. Time-delayed pulsation–translation model

The model is based on the following assumptions: (i) the bubbles remain spherical; (ii) thermal conduction and mass transfer are neglected; (iii) the inter-bubble distance is much larger than the bubble radii, $R_i/D_{ij} \ll 1$. The spherical-bubble assumption is adopted to isolate the effect of delayed pulsation–translation coupling. Consider three spherical bubbles in a compressible liquid with density ρ and sound speed c. The radius and position of bubble i are denoted by R_i and $\mathbf{p}_i$, respectively, and the inter-bubble distance is defined as $D_{ij} = |\mathbf{p}_j - \mathbf{p}_i|$. The pulsation–translation model is written as [26,39]:

$$\begin{aligned}\left(1-\frac{\dot{R}_i}{c}\right)R_i\ddot{R}_i+\left(\frac{3}{2}-\frac{\dot{R}_i}{2c}\right)\dot{R}_i^2-\frac{P_i}{\rho}\left(1+\frac{\dot{R}_i}{c}\right)-\frac{R_i}{\rho c}\frac{\mathrm{d}P_i}{\mathrm{d}t}\\ =\frac{\dot{\mathbf{p}}_i^2}{4}-\sum_{j=1,j\neq i}^{3}\left[\frac{R_j^2\ddot{R}_j+2R_j\dot{R}_j^2}{D_{ij}}\right.\\ \left.+(\mathbf{p}_i-\mathbf{p}_j)\cdot\frac{R_j^2\dot{\mathbf{p}}_i\dot{R}_j+R_j^3\ddot{\mathbf{p}}_j+5R_j^2\dot{R}_j\dot{\mathbf{p}}_j}{2D_{ij}^3}\right], i,j=1,2,3, i\neq j,\end{aligned} \tag{1}$$

$$\frac{R_i\ddot{\mathbf{p}}_i}{3}+\dot{R}_i\dot{\mathbf{p}}_i-\sum_{j=1,j\neq i}^{3}\left[\frac{\mathbf{p}_i-\mathbf{p}_j}{D_{ij}^3}\frac{\mathrm{d}(R_iR_j^2\dot{R}_j)}{\mathrm{d}t}\right]=\frac{F_{exi}}{2\pi\rho R_i^2}, i,j=1,2,3, i\neq j, \tag{2}$$

The effective pressure term P_i is taken in the form

$$P_i=\left(p_0+\frac{2\sigma}{R_{i0}}\right)\left(\frac{R_{i0}}{R_i}\right)^{3\gamma}-\frac{2\sigma}{R_i}-\frac{4\eta\dot{R}_i}{R_i}-p_0+p_a\sin\omega t, \tag{3}$$

where p_0 is the hydrostatic pressure, R_{i0} the ambient radius of the i-th bubble, γ the polytropic exponent of the gas within the bubbles, σ the gas-liquid interfacial surface tension at the bubble boundary, η the liquid viscosity, ω the circular frequency, and p_a the amplitude of the driving pressure. F_{exi} is the viscous drag and is expressed as [40]

$$\mathbf{F}_{exi}=-12\pi\eta R_i\left[\dot{\mathbf{p}}_i-\sum_{j=1,j\neq i}^{3}\frac{(\mathbf{p}_i-\mathbf{p}_j)R_j^2\dot{R}_j}{D_{ij}^3}\right]. \tag{4}$$

2.1. Incorporation of time delay

The pressure disturbance emitted by bubble j does not affect bubble i instantaneously. Instead, it propagates through the liquid at the sound speed c and reaches bubble i after a finite propagation time. Therefore, the state of bubble j entering the interaction with bubble i should be evaluated at the retarded time $t-\tau_{ij}$, where $\tau_{ij}=\frac{D_{ij}}{c}$ [37]. Incorporating

time-delay effects, we reformulate Eqs. (1) and (2) as follows:

$$\begin{aligned}
&\left(1-\frac{\dot{R}_i}{c}\right)R_i\ddot{R}_i+\left(\frac{3}{2}-\frac{\dot{R}_i}{2c}\right)\dot{R}_i^2-\frac{P_i}{\rho}\left(1+\frac{\dot{R}_i}{c}\right)-\frac{R_i}{\rho c}\frac{\mathrm{d}P_i}{\mathrm{d}t}\\
&\quad=\frac{\dot{\mathbf{p}}_i^2}{4}-\sum_{j=1,j\neq i}^{3}\left[\frac{R_j^2(t-\tau_{ij})\ddot{R}_j(t-\tau_{ij})+2R_j(t-\tau_{ij})\dot{R}_j^2(t-\tau_{ij})}{D_{ij}}\right.\\
&\quad\quad+(\mathbf{p}_i-\mathbf{p}_j)\cdot\frac{R_j^2(t-\tau_{ij})\dot{\mathbf{p}}_i\dot{R}_j(t-\tau_{ij})+R_j^3(t-\tau_{ij})\ddot{\mathbf{p}}_j(t-\tau_{ij})}{2D_{ij}^3}\\
&\quad\quad\left.+(\mathbf{p}_i-\mathbf{p}_j)\cdot\frac{5R_j^2(t-\tau_{ij})\dot{R}_j(t-\tau_{ij})\dot{\mathbf{p}}_j(t-\tau_{ij})}{2D_{ij}^3}\right],
\end{aligned}\tag{5}$$

$$\begin{aligned}
&\frac{R_i\ddot{\mathbf{p}}_i}{3}+\dot{R}_i\dot{\mathbf{p}}_i-\sum_{j=1,j\neq i}^{3}\left[\frac{\mathbf{p}_i-\mathbf{p}_j}{D_{ij}^3}\frac{\mathrm{d}(R_iR_j^2(t-\tau_{ij})\dot{R}_j(t-\tau_{ij}))}{\mathrm{d}t}\right]\\
&\quad=-\frac{6\eta}{\rho R_i}\left[\dot{\mathbf{p}}_i-\sum_{j=1,j\neq i}^{3}\frac{(\mathbf{p}_i-\mathbf{p}_j)R_j^2(t-\tau_{ij})\dot{R}_j(t-\tau_{ij})}{D_{ij}^3}\right].
\end{aligned}\tag{6}$$

In the denominators and geometric factors, D_{ij} and $\mathbf{p}_i-\mathbf{p}_j$ are evaluated at the current time t, whereas the source variables of bubble j are evaluated at $t-\tau_{ij}$. This approximation neglects the variation of the propagation path during the short delay time, which is consistent with the assumptions $|\dot{\mathbf{p}}_i|/c\ll 1$ and $R_i/D_{ij}\ll 1$. This treatment is consistent with retaining only $O(\tau_{ij})$ terms in the Taylor expansion. For a representative spacing $D_{ij}=200$ μm, sound speed $c=1500$ m/s, and driving frequency $f_0=20$ kHz, one obtains $\tau_{ij}\approx 1.33\times10^{-7}$ s, $\frac{\tau_{ij}}{T_0}\approx 2.7\times10^{-3}$, where $T_0=1/f_0$ is the acoustic period. Thus, the first-order delay approximation is asymptotically small for the parameter range considered here. The delayed variables are expanded around the current time t as

$$g_j(t-\tau_{ij})=g_j(t)-\tau_{ij}\dot{g}_j(t)+O(\tau_{ij}^2),\tag{7}$$

Here, g denotes any delayed source variable, including R, $\dot{R}$, $\ddot{R}$, $\dot{\mathbf{p}}$, and $\ddot{\mathbf{p}}$. Substituting Eqs. (7) into Eqs. (5) and (6) gives first-order correction terms proportional to D_{ij}/c. The resulting equations contain third-order derivatives such as $\dddot{R}_j$ and $\dddot{\mathbf{p}}_j$. Following the order-reduction procedure used for time-delayed bubble-interaction models [37,41], these higher-order derivatives are recast in terms of lower-order quantities. This procedure avoids introducing artificial high-order dynamics and retains only the accelerations $\ddot{R}_j$ and $\ddot{\mathbf{p}}_j$, which are determined self-consistently by the coupled pulsation–translation equations. Consequently, the final governing equations for pulsation and translation are obtained as:

$$\begin{aligned}
&\left(1-\frac{\dot{R}_i}{c}\right)R_i\ddot{R}_i+\left(\frac{3}{2}-\frac{\dot{R}_i}{2c}\right)\dot{R}_i^2-\frac{P_i}{\rho}\left(1+\frac{\dot{R}_i}{c}\right)-\frac{R_i}{\rho c}\frac{\mathrm{d}P_i}{\mathrm{d}t}\\
&\quad=\frac{\dot{\mathbf{p}}_i^2}{4}-\sum_{j=1,j\neq i}^{3}\left\{\frac{R_j^2\ddot{R}_j+2R_j\dot{R}_j^2}{D_{ij}}\right.\\
&\quad\quad-\frac{1}{c}\left[R_j\dot{R}_j\ddot{R}_j+\frac{\dot{R}_j^3}{2}+\frac{1}{\rho}\frac{\mathrm{d}(P_jR_j)}{\mathrm{d}t}+\frac{R_j\dot{\mathbf{p}}_j\cdot\ddot{\mathbf{p}}_j}{2}+\frac{\dot{R}_j\dot{\mathbf{p}}_j^2}{4}\right]\\
&\quad\quad+\frac{\mathbf{p}_i-\mathbf{p}_j}{2D_{ij}^3}\cdot\left(R_j^2\dot{\mathbf{p}}_i\dot{R}_j+R_j^3\ddot{\mathbf{p}}_j+5R_j^2\dot{R}_j\dot{\mathbf{p}}_j\right)\\
&\quad\quad-\frac{\mathbf{p}_i-\mathbf{p}_j}{2cD_{ij}^2}\cdot\left[R_j\dot{R}_j^2(2\dot{\mathbf{p}}_i+\dot{\mathbf{p}}_j)\right.\\
&\quad\quad+R_j^2(\dot{R}_j\ddot{\mathbf{p}}_j+2\ddot{R}_j\dot{\mathbf{p}}_j+\dot{\mathbf{p}}_i\ddot{R}_j)\\
&\quad\quad\left.\left.+\frac{3}{2\pi\rho R_j}\frac{\mathrm{d}(\mathbf{F}_{\eta j}R_j)}{\mathrm{d}t}\right]\right\},
\end{aligned}\tag{8}$$

$$
\begin{aligned}
&\frac{R_i\ddot{\mathbf{p}}_i}{3}+\dot{R}_i\dot{\mathbf{p}}_i-\sum_{j=1,j\neq i}^{3}\left\{\frac{\mathbf{p}_i-\mathbf{p}_j}{D_{ij}^3}\left(\dot{R}_iR_j^2\dot{R}_j+2R_iR_j\dot{R}_j^2+R_iR_j^2\ddot{R}_j\right)\right.\\
&\left.-\frac{\mathbf{p}_i-\mathbf{p}_j}{cD_{ij}^2}\left[\dot{R}_iR_j\left(2\dot{R}_j^2+R_j\ddot{R}_j\right)+R_i\left(\frac{\dot{R}_j^3}{2}+R_j\dot{R}_j\ddot{R}_j+\frac{1}{\rho}\frac{\mathrm{d}(P_jR_j)}{\mathrm{d}t}+\frac{R_j\dot{\mathbf{p}}_j\cdot\ddot{\mathbf{p}}_j}{2}\right)\right]\right\}\\
&=-\frac{6\eta}{\rho R_i}\left\{\dot{\mathbf{p}}_i-\sum_{j=1,j\neq i}^{3}\left[\frac{(\mathbf{p}_i-\mathbf{p}_j)R_j^2\dot{R}_j}{D_{ij}^3}-\frac{(\mathbf{p}_i-\mathbf{p}_j)(2R_j\dot{R}_j^2+R_j^2\ddot{R}_j)}{cD_{ij}^2}\right]\right\}.
\end{aligned}
\tag{9}
$$

where $\mathbf{F}_{\eta i}\approx -12\pi\eta R_i\dot{\mathbf{p}}_i$ is the leading-order Stokes drag approximation [40]. Compared with Eqs. (1) and (2), Eqs. (8) and (9) incorporate additional $O(1/c)$ terms that explicitly account for finite-speed acoustic propagation, i.e., time-delay effects. This formulation highlights that time delay acts as a perturbative modulation of the instantaneous pulsation–translation coupling rather than as an independent driving mechanism.

It is worth distinguishing the compressibility correction associated with the self-dynamics of an individual bubble from the additional radiation-damping contributions arising in a fully compressible inter-bubble interaction. The Keller–Miksis pulsation equation used here already accounts for the compressibility effects associated with the self-dynamics of each bubble, whereas the present formulation focuses on the retarded inter-bubble coupling due to the finite propagation time. For the representative parameters, $\omega D_{ij}/c$ is of order 10^{-2}, while $\omega R_i/c$ is of order 10^{-4}. These estimates indicate that finite propagation over the inter-bubble distance is associated with a larger characteristic compressibility scale in the present parameter regime. However, these two dimensionless scales alone do not provide a quantitative criterion for comparing radiation damping with time-delay effects, since the corresponding terms enter the governing equations with different derivative structures. A more complete treatment including both inter-bubble retardation and radiation-damping corrections, as considered by Thomas [37], is left for future work.

2.2. Analysis for spacing and orbital motion

The collective dynamics of a three-bubble cluster cannot be fully characterized by a single inter-bubble distance. To quantify both spacing regulation and orbital motion, we introduce the following analysis. The mean inter-bubble distance is $\bar{D}=\frac{D_{12}+D_{23}+D_{31}}{3}$. The spacing uniformity is quantified by the coefficient of variation,

$$
CV=\frac{\left(\frac{1}{3}\sum_{i<j}\left(D_{ij}-\bar{D}\right)^2\right)^{1/2}}{\bar{D}},i,j=1,2,3,i\neq j,
\tag{10}
$$

A smaller value of CV corresponds to more uniform spacing among the three pairwise distances. The centroid of the cluster is defined as

$$
\mathbf{X}_c=\frac{1}{3}\sum_{i=1}^{3}\mathbf{p}_i,
\tag{11}
$$

and the relative position of bubble i in the centroid frame is $\mathbf{r}_i=\mathbf{p}_i-\mathbf{X}_c$. For the two-dimensional motion considered here, $\mathbf{p}_i=(x_i,y_i)$ and $\mathbf{X}_c=(X_c,Y_c)$. Before differentiating, θ_i is unwrapped in time to avoid artificial jumps at $\pm\pi$. The angular coordinate of bubble i in the centroid frame is defined as

$$
\theta_i=\mathrm{atan2}\left(y_i-Y_c,x_i-X_c\right),
\tag{12}
$$

and the corresponding angular velocity is $\Omega_i=\frac{\mathrm{d}\theta_i}{\mathrm{d}t}$. The time-averaged angular velocity of the cluster is evaluated after the initial transient stage as

$$
\langle\Omega\rangle=\frac{1}{3}\sum_{i=1}^{3}\langle\Omega_i\rangle.
\tag{13}
$$

The sign of $\langle\Omega\rangle$ determines the rotational direction, whereas its magnitude determines the orbital period, $T_{\mathrm{orb}} = \frac{2\pi}{|\langle\Omega\rangle|}$.

To quantify the influence of time delay, two simulations are compared for each parameter set: one using the instantaneous-interaction model and the other using the time-delayed model. The delay-induced change in the selected spacing is measured by

$$\delta_{\bar{D}} = \frac{\bar{D}_{\mathrm{delay}} - \bar{D}_{\mathrm{no-delay}}}{\bar{D}_{\mathrm{no-delay}}}, \tag{14}$$

and the delay-induced change in spacing uniformity is measured by

$$\delta_{CV} = \frac{CV_{\mathrm{delay}} - CV_{\mathrm{no-delay}}}{CV_{\mathrm{no-delay}}}. \tag{15}$$

To provide analysis quantities for the mode-selective modulation discussed below, the translational acceleration is further projected onto the radial and tangential directions in the centroid frame. The radial unit vector is $\mathbf{e}_{r,i} = \frac{\mathbf{r}_i}{|\mathbf{r}_i|}$, and the tangential unit vector is taken as $\mathbf{e}_{\theta,i} = (-e_{r,i,y}, e_{r,i,x})$.

The translational acceleration $\mathbf{a}_i$ is projected onto the radial and tangential directions as $a_{r,i} = \mathbf{a}_i \cdot \mathbf{e}_{r,i}, a_{\theta,i} = \mathbf{a}_i \cdot \mathbf{e}_{\theta,i}$. In component form, these quantities are

$$a_{r,i} = \frac{\ddot{x}_i(x_i - X_c) + \ddot{y}_i(y_i - Y_c)}{\sqrt{(x_i - X_c)^2 + (y_i - Y_c)^2}}, \tag{16}$$

and

$$a_{\theta,i} = \frac{-\ddot{x}_i(y_i - Y_c) + \ddot{y}_i(x_i - X_c)}{\sqrt{(x_i - X_c)^2 + (y_i - Y_c)^2}}. \tag{17}$$

The cluster-averaged radial and tangential acceleration magnitudes are defined as

$$A_r = \frac{1}{3}\sum_{i=1}^{3} |a_{r,i}|, \tag{18}$$

and

$$A_\theta = \frac{1}{3}\sum_{i=1}^{3} |a_{\theta,i}|. \tag{19}$$

Here, A_r measures the strength of the radial spacing-regulation tendency, whereas A_θ measures the strength of the tangential rotational tendency around the centroid. The quantities $\langle A_r\rangle$ and $\langle A_\theta\rangle$ denote the long-time averaged values of A_r and A_θ evaluated after the initial transient stage. The bubbles are assumed to remain spherical throughout their oscillations to describe the pulsation-translation coupling considered in this study. This assumption has certain limitations under strong acoustic forcing, particularly during the violent collapse stage, where non-spherical deformation may occur. Such effects can modify the interactions between bubbles and may affect the tangential acceleration. Therefore, the results obtained in this study should be interpreted within the framework of the spherical-bubble assumption. A fully deformable bubble model would be required to quantitatively assess these effects, which will be considered in future work.

The governing equations are solved numerically using MATLAB. The coupled algebraic system for $\ddot{R}_i$ and $\ddot{\mathbf{p}}_i$ was solved at each time step. The resulting first-order system was integrated using ODE45. The relative and absolute tolerances were 1×10^{-8} and 1×10^{-11}, respectively. The three bubbles are arranged in an equilateral triangle with an initial spacing of 200 μm. The physical parameters are chosen as follows: liquid density $\rho = 998$ kg/m^3, sound speed $c = 1500$ m/s, surface tension $\sigma = 0.0725$ N/m, dynamic viscosity $\eta = 0.001$ Pa $\cdot$ s, polytropic exponent $\gamma = 1.4$, ambient pressure $p_0 = 1$ bar, and driving frequency $f_0 = 20$ kHz. The acoustic angular frequency is $\omega = 2\pi f_0$. The initial bubble radii are chosen in the micrometer range, $R_{i0} \leq 10$ μm [42], consistent with cavitation-bubble conditions considered in the present study.

3. Delay-free collective modes and their time-delay modulation

3.1. Representative collective states and mode-selective modulation

We first examine two representative collective states to distinguish the effect of time delay on spacing regulation from its effect on orbital motion. Figure 1 shows an orbital constant-distance state of the three-bubble cluster. In the delay-free model, the centroid-frame trajectories form repeated closed loops, indicating that the bubbles rotate around the centroid while maintaining a bounded relative configuration. This orbital behavior is further confirmed by the unwrapped angular displacement in Fig. 1(c), which accumulates by about 5.0 rad over 500 acoustic cycles.

After the time-delay is considered, the bounded finite-distance configuration is preserved, but the orbital component is strongly weakened. As shown in Fig. 1(b), the centroid-frame trajectories remain confined, whereas the delayed angular displacement in Fig. 1(c) accumulates by only about 1.2 rad over the same time interval. The spacing analysis in Fig. 1(d) shows that the mean inter-bubble distance increases from about 85.6 μm to about 112.5 μm, while the coefficient of variation increases from about 0.33 to about 0.41. The pairwise inter-bubble distances shown in Figs. 1(e) and 1(f) further confirm that the distances between all bubble pairs increase when the time delay is included. Thus, time delay does not destroy the ordered cluster, but selects a larger and slightly less uniform configuration while reducing its orbital rotation.

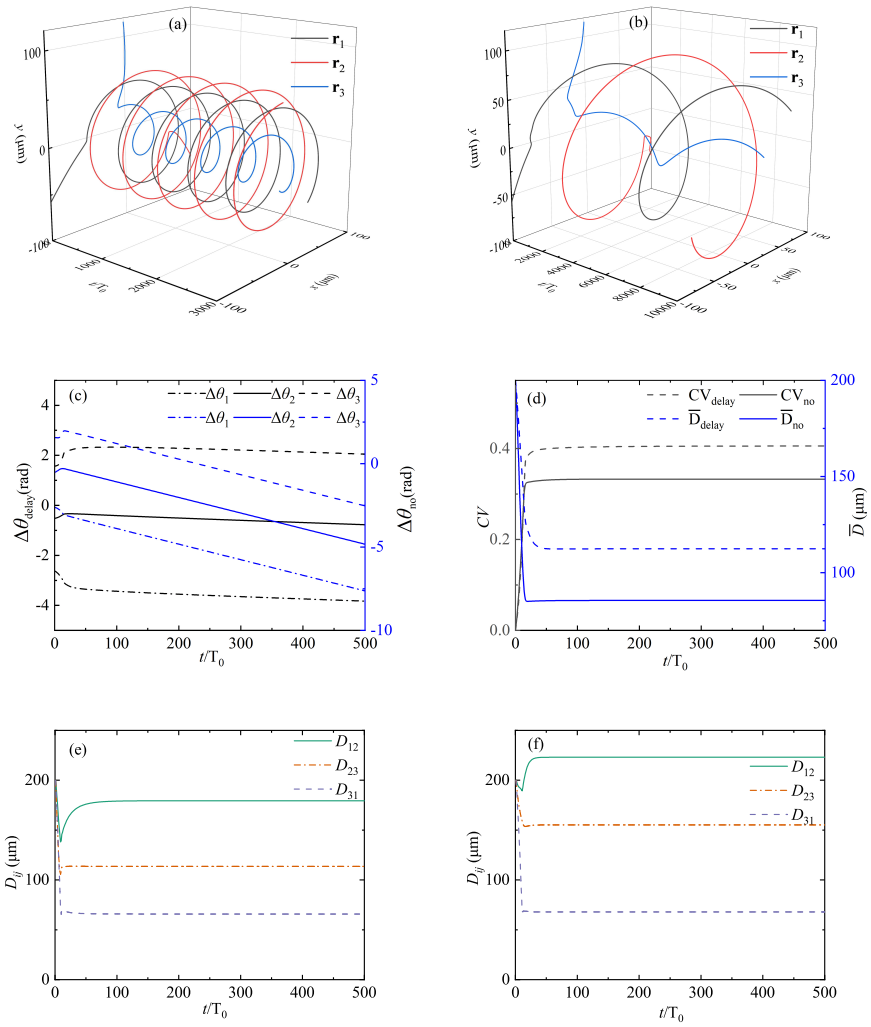


Figure 1: Orbital constant-distance state of the three-bubble cluster with $R_{10} = 4.2$ μm, $R_{20} = 4.9$ μm, and $R_{30} = 6$ μm at $p_a = 1.16$ bar. (a) Centroid-frame trajectories $\mathbf{r}_i$ without delay. (b) Centroid-frame trajectories $\mathbf{r}_i$ with delay. (c) Unwrapped angular displacements $\Delta\theta_i$. (d) CV and $\bar{D}$ comparison, left CV, right $\bar{D}$. (e) Pairwise inter-bubble distances without delay. (f) Pairwise inter-bubble distances with delay.

All quantities reported in Tables 1–4 were evaluated after 500 acoustic cycles, using the final 100 cycles for analysis to exclude the initial transient response. This separation between spacing regulation and orbital rotation is clarified by the acceleration analysis. As shown in Table 1, the long-time averaged radial acceleration remains of the same order after time delay is introduced, changing from 1.49×10^7 m/s^2 to 1.24×10^7 m/s^2. Therefore, the radial component needed to maintain finite spacing remains effective. By contrast, the tangential acceleration decreases from 4.73×10^6 m/s^2 to 1.06×10^6 m/s^2, only about 22% of the delay-free value. Consistently, $|\langle\Omega\rangle|$ decreases from 186.99 rad/s to 17.21 rad/s. The cluster therefore remains bounded because radial regulation is retained, whereas its orbital motion is weakened because tangential driving is strongly reduced.

The phase analysis in Table 2, obtained from the same analysis window, provides further support for this interpretation. The relative phase was computed as the principal wrapped phase difference, $\Delta\phi_i = \arg\left[\exp\left(i(\phi_{a_{\theta i}} - \phi_{\dot{R}_i})\right)\right]$, which confines $\Delta\phi_i$ to $[-\pi, \pi]$ and removes the arbitrary 2π branch ambiguity. Time delay modifies the phase relation between radial pulsation velocity and tangential acceleration in a bubble-dependent manner. Bubble b_1 undergoes the largest phase

change, whereas b_2 and b_3 show much smaller changes. The mean absolute phase change is approximately 0.50 rad. This bubble-dependent phase modulation reduces the coherence of the tangential acceleration in the centroid frame, consistent with the marked decrease in $|\langle\Omega\rangle|$.

Table 1: Long-time averaged acceleration and rotation analysis for the orbital state shown in Fig. 1.

Quantity	No delay	Delay	Ratio
$\langle A_r\rangle(\mathrm{m/s^2})$	1.49×10^7	1.24×10^7	0.83
$\langle A_\theta\rangle(\mathrm{m/s^2})$	4.73×10^6	1.06×10^6	0.22
$\lvert\langle\Omega\rangle\rvert(\mathrm{rad/s})$	186.99	17.21	0.09

Table 2: Phase difference between radial pulsation velocity and tangential acceleration shown in Fig. 1.

Bubble	No delay (rad)	Delay (rad)	Phase shift (rad)
b_1	2.84	-2.09	1.35
b_2	0.81	0.84	0.03
b_3	-1.77	-1.90	-0.13
Mean $\lvert\Delta\phi\rvert$	–	–	0.50

Figure 2 shows another finite-distance collective state. In the delay-free model, the centroid-frame trajectories remain bounded and retain a weak orbital component. After the time-delay is considered, the centroid-frame trajectories remain bounded but become nearly rectilinear, indicating that the orbital component is strongly suppressed. The spacing analysis in Figs. 2(c) and 2(d) again shows a statistically steady finite-distance state, with a larger spacing and a slightly increased coefficient of variation in the delayed model.

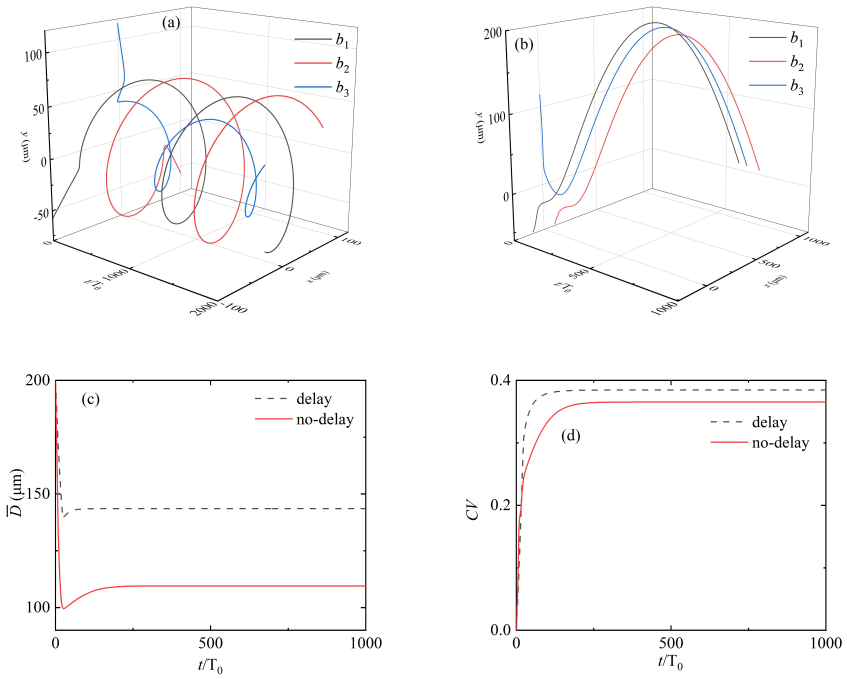


Figure 2: Time-delay modulation of the constant-distance translation for the three-bubble cluster with $R_{10} = 4.2$ μm, $R_{20} = 5$ μm, and $R_{30} = 6.3$ μm at $p_a = 1.16$ bar. (a) Centroid-frame trajectories $\mathbf{r}_i$ without delay. (b) Centroid-frame trajectories $\mathbf{r}_i$ with delay. (c) Comparison of the mean inter-bubble distance between the delay-free and delayed models. (d) Comparison of the coefficient of variation between the delay-free and delayed models.

The acceleration analysis for this case demonstrates the same radial–tangential separation more clearly. As listed in Table 3, $\langle A_r \rangle$ changes only slightly from 1.15×10^7 m/s^2 to 1.16×10^7 m/s^2, indicating that the radial spacing-regulation component is essentially preserved. By contrast, $\langle A_\theta \rangle$ decreases from 4.80×10^6 m/s^2 to 3.16×10^4 m/s^2, corresponding to only about 0.7% of the delay-free value. Consistently, $|\langle \Omega \rangle|$ decreases from 114.21 rad/s to 0.92 rad/s. Thus, the delayed state approaches rectilinear relative motion because the tangential driving is almost suppressed while the radial component remains active. The phase analysis in Table 4 further shows bubble-dependent phase shifts, with a mean absolute phase change of approximately 0.44 rad. This phase detuning is consistent with reduced coherence of the tangential acceleration among the three bubbles and with the near cancellation of the orbital component.

Table 3: Long-time averaged acceleration and rotation analysis for the case shown in Fig. 2.

Quantity	No delay	Delay	Ratio
$\langle A_r \rangle$(m/s^2)	1.15×10^7	1.16×10^7	1.01
$\langle A_\theta \rangle$(m/s^2)	4.80×10^6	3.16×10^4	0.007
$\lvert\langle \Omega \rangle\rvert$(rad/s)	114.21	0.92	0.008

Table 4: Phase difference between radial pulsation velocity and tangential acceleration for the case shown in Fig. 2.

Bubble	No delay (rad)	Delay (rad)	Phase shift (rad)
b_1	-0.37	-1.10	-0.73
b_2	0.75	0.79	0.04
b_3	-1.24	-1.80	-0.56
Mean $\lvert\Delta\phi\rvert$	–	–	0.44

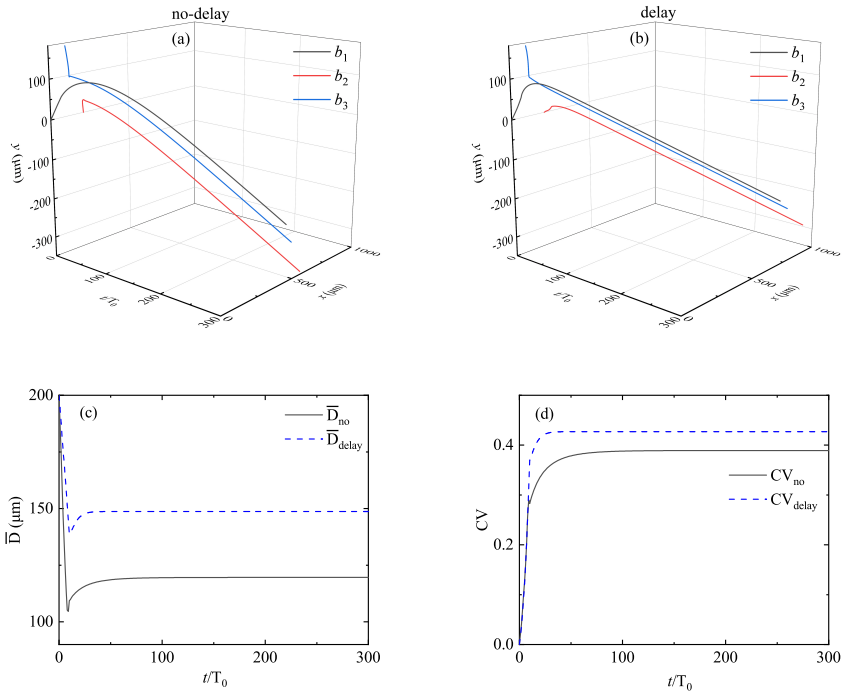


Figure 3: Robustness of rectilinear collective translation for the three-bubble cluster with $R_{10} = 4.2$ μm, $R_{20} = 5$ μm, and $R_{30} = 6.3$ μm at $p_a = 1.17$ bar. (a) Absolute trajectories without delay. (b) Absolute trajectories with delay. (c) Comparison of the mean inter-bubble distance between the delay-free and delayed models. (d) Comparison of the coefficient of variation between the delay-free and delayed models.

As shown in Fig. 3, the absolute trajectories in both the delay-free and delayed models indicate that the three bubbles move as a cluster. The delayed model selects a larger inter-bubble spacing, consistent with the trend reported for the two-bubble system [38]. These representative cases therefore show that time delay mainly shifts the spatial scale and suppresses the orbital component of the finite-distance state. Previous studies have also shown that finite propagation time can significantly influence coupled-bubble dynamics. Doinikov et al. [43] showed that incorporating finite propagation time improves the agreement between the coupled-bubble theory and previously reported experimental measurements of collective bubble dynamics. Ooi et al. [35] similarly found that including time delay improves agreement with experiments for a linear bubble chain and that its effect on different collective modes becomes stronger for more closely spaced bubbles. These findings provide the physical relevance of incorporating finite propagation time in the present model.

To further examine the robustness of the rectilinear collective translation with respect to the initial bubble configuration, we consider a non-equilateral triangular arrangement with the initial bubble positions given by $(0,0)$, $(200\ \mu\text{m}, 0)$, and $(50\ \mu\text{m}, 200\ \mu\text{m})$. All other parameters are the same as those in Fig. 3. As shown in Fig. 4(a), the three bubbles still

exhibit rectilinear collective translation despite the change in the initial configuration. Meanwhile, the mean inter-bubble distance $\bar{D}$ and coefficient of variation CV remain unchanged in Fig. 4(b). This indicates that both the collective translating state and its characteristic spatial organization are robust to the initial bubble configuration considered here.

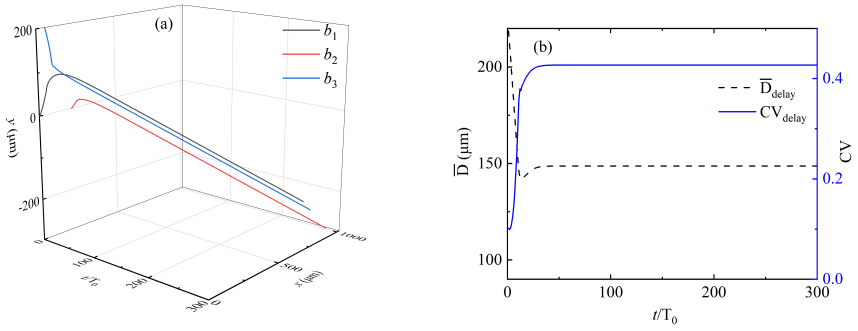


Figure 4: Robustness of rectilinear collective translation for the three-bubble cluster with $R_{10} = 4.2$ μm, $R_{20} = 5$ μm, and $R_{30} = 6.3$ μm at $p_a = 1.17$ bar, with a non-equilateral initial configuration. (a) Absolute trajectories. (b) Comparison of CV (right axis) and $\bar{D}$ (left axis).

3.2. Dependence on the driving acoustic pressure

The representative cases above indicate that the selected collective state depends on both acoustic pressure and initial bubble radii. We therefore examine the pressure dependence for $R_{10} = 4.2$ μm, $R_{20} = 5$ μm, and $R_{30} = 6.3$ μm over a pressure interval in which finite-distance collective motion is maintained. Figure 5(a) shows that the delay-induced spacing change, $\delta_{\bar{D}}$, remains positive throughout the pressure interval. Thus, the delayed model consistently selects a larger mean inter-bubble distance than the delay-free model. The magnitude of $\delta_{\bar{D}}$ decreases from approximately 0.40 near $p_a = 1.160$ bar to about 0.24 in the middle of the interval, and then increases slightly as p_a approaches 1.175 bar. The delay-induced spacing modulation is therefore robust, although it is not strictly monotonic with pressure.

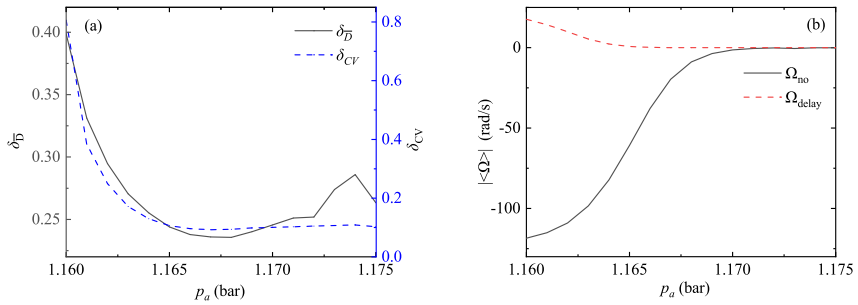


Figure 5: Dependence of the delay-induced modulation on the driving acoustic pressure for the three-bubble cluster with $R_{10} = 4.2$ μm, $R_{20} = 5$ μm, and $R_{30} = 6.3$ μm. (a) Relative changes in the mean inter-bubble distance $\delta_{\bar{D}}$ and coefficient of variation δ_{CV}. (b) Comparison of the mean angular velocity $|\langle\Omega\rangle|$ between the delay-free and delayed models.

The change in spacing uniformity, δ_{CV}, is also positive over the whole pressure interval, showing that the delayed model generally produces a less uniform configuration. At lower pressure, δ_{CV} is larger, indicating that the finite-distance configuration is more sensitive to the delay correction. As the pressure increases, δ_{CV} decreases and approaches a smaller

nearly saturated value. This suggests that stronger pulsation–translation coupling helps maintain spacing regulation, although time delay still shifts the selected configuration.

Figure 5(b) shows the corresponding mean angular velocity. In the delay-free model, $|\langle\Omega\rangle|$ is relatively large at lower pressures and decreases as the pressure increases. After time delay is introduced, $|\langle\Omega\rangle|$ remains substantially smaller over almost the entire pressure range. The persistence of finite spacing together with the reduction of angular velocity confirms that the mode-selective delay effect is not restricted to a single representative trajectory.

3.3. Dependence on the initial radius

We finally examine the dependence on the initial bubble radii at fixed $R_{10} = 4.2\ \mu$m and $p_a = 1.17$ bar. Figure 6 shows the delay-induced changes in mean spacing and spacing uniformity as R_{20} and R_{30} are varied. As shown in Fig. 6(a), $\delta_{\bar{D}}$ remains positive over the whole scanned region. Therefore, for all radius combinations considered here, time delay selects a larger mean inter-bubble distance. The value of $\delta_{\bar{D}}$ lies approximately between 0.20 and 0.40, indicating a substantial spacing enlargement. However, the distribution is not monotonic with either R_{20} or R_{30}. Instead, regions with stronger spacing modulation appear as band-like structures. This indicates that the delay effect is governed not simply by bubble size, but by radius-dependent pulsation phases and the resulting translation coupling among the three bubbles.

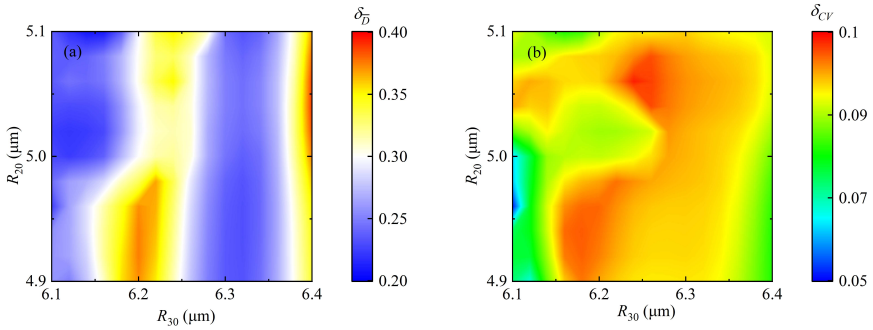


Figure 6: Dependence of the delay-induced modulation on the initial radii at $R_{10} = 4.2\ \mu$m and $p_a = 1.17$ bar. (a) Relative change in the mean inter-bubble distance, $\delta_{\bar{D}}$. (b) Relative change in the coefficient of variation, δ_{CV}.

Figure 6(b) shows that δ_{CV} is also positive throughout the radius plane. Thus, time delay generally reduces the spacing uniformity of the three-bubble configuration. Compared with $\delta_{\bar{D}}$, however, the variation range of δ_{CV} is smaller, approximately from 0.05 to 0.10. The dominant effect of time delay is therefore to shift the selected mean spacing, while the loss of spacing uniformity is more moderate.

Overall, the pressure and radius scans lead to the same conclusion as the representative cases. Time delay robustly increases the selected spacing and tends to reduce spacing uniformity in the examined finite-distance regime. The non-monotonic parameter dependence indicates that the delay effect is controlled not simply by bubble size or acoustic pressure, but by the parameter-dependent pulsation amplitudes, collapse phases, and phase-weighted translational interactions among the three bubbles.

4. Conclusions

A time-delayed pulsation–translation model was developed to investigate finite-distance collective dynamics in a three-bubble acoustic cluster. The non-collinear three-bubble configuration supports both radial spacing regulation and tangential orbital motion, allowing the influence of acoustic time delay on different collective degrees of freedom to be distinguished.

The results show that time delay does not independently generate the bounded or orbital states. Instead, it modifies the states already supported by nonlinear pulsation–translation coupling. In the representative cases, the delayed cluster remains spatially bounded but selects a larger mean inter-bubble spacing and a moderately less uniform configuration.

The radial–tangential acceleration decomposition reveals a mode-selective response. The radial component remains of the same order of magnitude and therefore continues to regulate the finite-distance configuration. By contrast, the tangential component and its phase coherence are strongly weakened. Consequently, the accumulated angular displacement and mean angular velocity decrease markedly, and an orbital state may approach nearly rectilinear collective motion.

Pressure and initial-radius scans further show that the spacing enlargement persists throughout the examined finite-distance regime, although its magnitude varies non-monotonically with the driving pressure and bubble-size combination. These results identify finite-speed acoustic propagation as a mode-selective perturbation: radial confinement is comparatively robust, whereas sustained orbital motion is more sensitive to the phase changes introduced by retarded coupling.

Acknowledgments

This work was supported by the National Natural Science Foundation of China (Nos. 12074185 and 12264008), and foundation of the State Key Laboratory of Acoustics and Marine Information, Institute of Acoustics, Chinese Academy of Sciences (No. SKLA202616).

References

[1] Chen W Z 2014 *Acoustic cavitation physics* (Science Press)

[2] Flannigan D J and Suslick K S 2005 *Nature* **434** 52

[3] Church C C 1989 *J. Acoust. Soc. Am.* **86** 215

[4] Supponen O, Obreschkow D, Kobel P, Tinguely M, Dorsaz N and Farhat M 2017 *Phys. Rev. Fluids* **2** 093601

[5] Elder S A 1959 *J. Acoust. Soc. Am.* **31** 54

[6] Doinikov A A and Bouakaz A 2010 *J. Acoust. Soc. Am.* **127** 703

[7] Hiller R A, Putterman S J and Weninger K R 1998 *Phys. Rev. Lett.* **80** 1090

[8] Miller M W, Miller D L and Brayman A A 1996 *Ultrasound in Medicine and Biology* **22** 1131

[9] Mason T J 2016 *Ultrasonics Sonochemistry* **29** 519

[10] Lamminen M O, Walker H W and Weavers L K 2004 *J. Membr. Sci.* **237** 213

[11] Prentice P, Cuschieri A, Dholakia K, Prausnitz M and Campbell P 2005 *Nat. Phys.* **1** 107

[12] Chen W S, Matula T J, Brayman A A and Crum L A 2003 *J. Acoust. Soc. Am.* **113** 643

[13] Parlitz U, Scheffczyk C, Akhatov I and Lauterborn W 1995 *Chaos Solitons Fractals* **5** 1881

[14] Mettin R, Luther S, Ohl C D and Lauterborn W 1999 *Ultrason. Sonochem.* **6** 25

[15] Doinikov A A and Zavtrak S T 1996 *J. Acoust. Soc. Am.* **99** 3849

[16] Lauterborn W, Kurz T, Geisler R, Schanz D and Lindau O 2007 *Ultrason. Sonochem.* **14** 484

[17] Dubus B, Moussatov A, Granger C, Campos-Pozuelo C and Lauterborn W 2004 *J. Acoust. Soc. Am.* **116** 2542

[18] Kobelev Y A, Ostrovskii L A and Sutin A M 1979 *Pis'ma Zh. Eksp. Teor. Fiz.* **30** 423

[19] Marston P, Trinh E, Depew J and Asaki J 1994 *in Bubble Dynamics and Interface Phenomena, edited by J.R. Blake* (Kluwer Academic)

[20] Shirota M, Yamashita K and Inamura T 2012 *Nonlinear Acoust.* **1474** 155

[21] Desjouy C, Labelle P, Gilles B, Bera J C and Inserra C 2013 *Phys. Rev. E* **88** 033006

[22] Desjouy Cand Labelle P, Gilles B, Bera J C and Inserra C 2013 *J. Acoust. Soc. Am.* **133** 3277

[23] Bai L, Sun J, Gao Y, Xu W, Zeng Z, Ma Y and Bai L 2021 *Ultrason. Sonochem.* **74** 105577

[24] Doinikov A A 1999 *Phys. Rev. E* **59** 3016

[25] Doinikov A A 2001 *Phys. Rev. E* **64** 026301

[26] Doinikov A A 2004 *J. Acoust. Soc. Am.* **116** 821

[27] Barbat T and Ashgriz N 2004 *Appl. Math. Comput.* **157** 775

[28] Pelekasis N A, Gaki A, Doinikov A and Tsamopoulos J A 2004 *J. Fluid Mech.* **500** 313

[29] Zhang L and Chen W 2024 *Ultrasonics Sonochemistry* **110** 107050

[30] Luther S and Allen J S 1999 *J. Acoust. Soc. Am.* **105** 1145

[31] Heckman C, Sah S and Rand R 2010 *Commun. Nonlinear Sci. Numer. Simul.* **15** 2735

[32] Wang Q, Han Z, Zhang X and Yang Y 2021 *Chaos Solitons Fractals* **148** 111053

[33] Heckman C and Rand R 2013 *Nonlinear Dyn.* **71** 121

[34] Coulombel P and Denner F 2024 *Phys. Fluids* **36**

[35] Ooi A, Nikolovska A and Manasseh R 2008 *J. Acoust. Soc. Am.* **124** 815

[36] Thomas D C, Ilinskii Y A, Zabolotskaya E and Hamilton M F 2011 Modeling time delay in clusters of interacting bubbles *Proceedings of Meetings on Acoustics* vol 12 p 045005

[37] Thomas D C 2012 *Stability and dynamics of systems of interacting bubbles with time-delay and self-action due to liquid compressibility* Ph.D. thesis The University of Texas at Austin Austin

[38] Zhang L, Wang X and Liang J 2026 *Phys. Fluids* **38** 043328

[39] Keller J B and Miksis M 1980 *J. Acoust. Soc. Am.* **68** 628

[40] Levich B V 1962 *Physicochemical Hydrodynamics* (Englewood Cliffs, NJ: Prentice-Hall)

[41] Prosperetti A and Lezzi A 1986 *J. Fluid Mech.* **168** 457

[42] Mettin R, Akhatov I, Parlitz U, Ohl C D and Lauterborn W 1997 *Phys. Rev. E* **56** 2924

[43] Doinikov A A, Manasseh R and Ooi A 2005 *The Journal of the Acoustical Society of America* **117** 47